International Journal of Multiphase Flow 35 (2009) 946–951

Contents lists available at ScienceDirect

International Journal of Multiphase Flow

journal homepage: www.elsevier.com/locate/ijmulflow

Enhancement of the critical heat flux in saturated pool boiling using honeycomb porous media

Shoji Mori *, Kunito Okuyama

Department of Chemical Engineering Science, Yokohama National University, 79-5 Tokiwadai, Hodogaya-ku, Yokohama 240-8501, Japan

ARTICLE INFO

Article history:
Received 22 December 2008
Received in revised form 25 April 2009
Accepted 8 May 2009
Available online 18 May 2009

Keywords:
Pool boiling
Critical heat flux
Porous media
Capillary force

ABSTRACT

Enhancement of the critical heat flux in pool boiling by the attachment of a honeycomb-structured porous plate on a heated surface is investigated experimentally using water under saturated boiling conditions. As the height of the honeycomb porous plate on the heated surface decreases, the CHF increases to 2.5 MW/m^2, which is approximately 2.5 times that of a plain surface (1.0 MW/m^2). Automatic liquid supply due to capillary action and reduction of the flow resistance for vapor escape due to the separation of liquid and vapor flow paths by the honeycomb-structure are verified to play an important role in the enhancement of the CHF. A simplified one-dimensional model for the capillary suction limit, in which the pressure drops due to liquid and vapor flow in the honeycomb porous plate balances the capillary force, is applied to predict the CHF. The calculated results are compared with the measured results.

1. Introduction

Pool boiling has been used for cooling in numerous thermal energy dissipation systems because of its high heat removal capacity and the liquid being supplied to the heated surface without a pump. The enhancement of the heat-transfer coefficient and the critical heat flux (CHF) under pool boiling conditions is still under investigation. For example, various surface modifications, including integrated surface structures such as channels and fins, and the coating of a porous layer onto the heat transfer surface, have been shown to effectively enhance the boiling heat transfer (Bar-Cohen, 1993; Honda and Wei, 2004; Lienhard et al., 1973; Coursey et al., 2005). The coating of a thin porous layer of uniform thickness onto boiling surfaces has been experimentally proven to be an effective technique to increase the CHF and reduce the surface superheat for a given surface heat flux in comparison with a plain surface (Webb, 1983; Mugha and Plumb, 1996; Chang and You, 1997; Hwang and Kaviany, 2006; Arik et al., 2007). In general, the CHF on the surface with a thin and uniform coating of a porous layer is enhanced to approximately twice that of a plain surface (Hwang and Kaviany, 2006; Liter and Kaviany, 2001). Boiling heat transfer on porous layer coated surfaces may be augmented due to nucleation from numerous sites, evaporation inside the pore structure, vapor ejection, and liquid suction from the top surface of the porous layer. With the increase in the surface heat flux, the flow rates of liquid and vapor through the porous layer increase. The increased flow resistance inside the porous layer may cause the formation and extension of a vapor layer near the heated surface, which may result in the transition from nucleate to film boiling.

Several researchers have offered novel structures of the porous media in which the liquid and vapor flow paths will be separated. Such separation of the flow path may reduce flow resistance and, as the result, increase the CHF.

Malyshenko (1991) was the first to experimentally investigate the boiling curves for the surface on which the porous layer with vapor escape channels is coated. Stubos and Buchlin (1999) examined analytically the effect of vapor channels traversing the porous layer on the CHF. Semenic et al. (2008) dissipated 4.9 MW/m^2 in pool boiling at a superheat of 128 K using a bi-porous wick that consists of clusters of fine powder. Micro-pores inside the clusters continuously supply the working liquid to the surface of the clusters where the evaporation takes place, while macro-pores between the clusters allow for easy escape of vapor. Note that the geometric surface area of the bi-porous wick (2552 mm^2) was much larger than the heated surface area (71 mm^2) (Semenic et al., 2008). The effect of the porous layer on the CHF enhancement may depend on the diameter of the porous layer relative to that of the heated surface because liquid may be pumped toward the center of the heated surface along the surface due to capillary suction. Wu et al. (2002) showed experimentally the effects of the size and density of vapor channels on pool boiling heat transfer. The CHF, however, has not been enhanced more than the effect of an extended surface area.

Liter and Kaviany (2001) showed that modulated (periodically non-uniform thickness) porous layer coating enhances the pool boiling critical heat flux of pentane by nearly three times

* Corresponding author. Tel.: +81 45 339 4010; fax: +81 45 339 4005.
E-mail addresses: morisho@ynu.ac.jp (S. Mori), okuyama@ynu.ac.jp (K. Okuyama).

0301-9322/$ - see front matter © 2009 Elsevier Ltd. All rights reserved.
doi:10.1016/j.ijmultiphaseflow.2009.05.003

(0.76 MW/m^2) that of a plain surface (0.25 MW/m^2). Two possible liquid choking limits, that is, the hydrodynamic limit and the viscous-drag limit were proposed as mechanisms by which to determine the CHF. For the tested surface coating and fluid system, the measured CHFs were in good agreement with the predicted CHFs based on the hydrodynamic limit, where Zuber's hydrodynamic theory is modified to account for the effect of the coating modulation wavelength on the development of the stable vapor layer above the coated surface.

Based on the studies mentioned above, the mechanism of the CHF enhancement by use of porous media will be explained by combinations of the capillary suction effect, the extended surface area effect, and the effect of the decrease in the flow-critical length scale or the decrease in the distance between the vapor columns, which is regulated by the modulation of the porous layer as suggested by Liter and Kaviany (2001).

In most experimental studies, the porous layer was prepared on the test surface by spraying or sintering metal particles of the order of several dozen to hundreds of microns, which may provide relatively large micro-pores that are not small enough to cause large capillary suction. In addition, it will be difficult to evaluate each of the effects of the capillary suction and the extended surface area on the CHF enhancement.

We focus on the effect of the capillary suction on the enhancement of the CHF and its intensification. A honeycomb-structured ceramic porous plate, which is commercially available as a filter for purifying exhaust gases from combustion engines, was selected as the porous material. This honeycomb porous plate has considerably small micro-pores on the order of 0.1 μm, as compared with those of sintered metal powders and is simply attached to the test surface without any treatment, such as spraying or sintering. As mentioned above, the keys for the CHF enhancement by the porous layer will be the automatic liquid supply due to capillary action and the reduction of the vapor escape flow resistance due to the separation of the liquid and vapor flow paths. Macro-pores of the honeycomb porous plate serve as the channels for vapor to escape from the heated surface, and suppress the pressure increase in the porous layer due to vapor generation. Since the thermal conductivity of ceramic material is much lower than that of the porous layer made of metal, the capillary suction effect on the CHF enhancement will be evaluated appropriately using this ceramic porous plate. As a result of the experiment, the CHF of water under the saturated pool boiling conditions at atmospheric pressure is shown to increase to 2.5 MW/m^2, which is approximately 2.5 times that of a plain surface (1.0 MW/m^2). A simplified one-dimensional model for the capillary limit, in which the pressure drops caused by liquid and vapor flow through the honeycomb porous plate balance the capillary force, is applied to predict the CHF. The calculated results are compared with the observed results.

2. Experimental apparatus and procedure

2.1. Experimental apparatus

A schematic diagram of the pool boiling test facility is shown in Fig. 1. The main vessel made of Pyrex glass has an inner diameter of 87 mm and a height of 200 mm. The pool container was filled with distilled water to a height above the heated surface of approximately 60 mm. The heater component was a copper cylinder having a diameter of 32 mm and a height of 100 mm. The heat flux was supplied to the boiling surface through a copper cylinder using a cartridge electric heater, which was inserted into the copper cylinder and was controlled by an AC voltage regulator. The heat loss from the sides and bottom of the copper cylinder was reduced using a ceramic fiber insulation material.

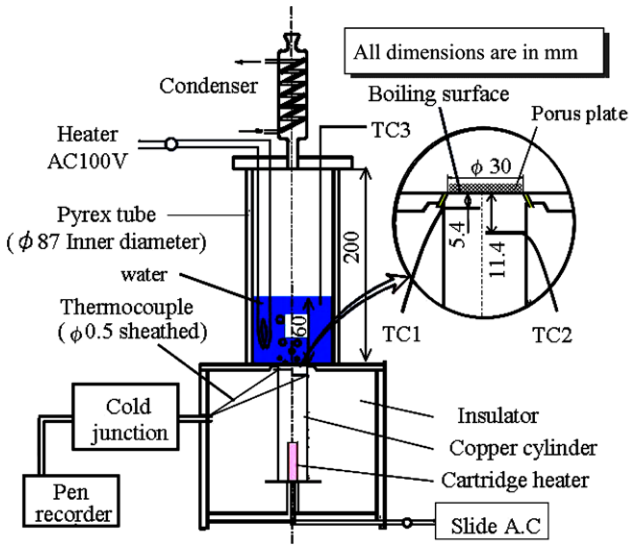

Fig. 1. Schematic diagram of the experimental apparatus.

The top horizontal surface of the copper cylinder with a diameter of 30 mm is smooth and is used as the heat transfer surface in the experiments. Two sheathed thermocouples with an outer diameter of 0.5 mm were inserted horizontally to the center line of the copper cylinder. The thermocouples (TC1 and TC2 shown in Fig. 1) in the copper cylinder were set apart axially by 6.0 mm. The closest thermocouple to the surface was located 5.4 mm below the boiling surface. These thermocouples were calibrated using a platinum resistance thermometer. The wall temperature and the wall heat flux were calculated by applying the Fourier's Law, where the thermal conductivity of the copper was evaluated at the arithmetic averaged temperature between TC1 and TC2.

2.2. Experimental procedure

Experiments were carried out using distilled water as a working fluid under saturated conditions at atmospheric pressure. A sheathed heater was installed above the heated surface in the liquid bath in order to keep the liquid temperature at the saturation temperature. At each run, the heat flux was increased in increments of approximately 0.1 MW/m^2 until burnout occurred. All of the measurements were performed at the steady state. The steady state was regarded as being reached when the temperatures did not change more than 0.25 K for at least 10 min. When burnout occurred, the heating was immediately stopped in order to prevent the heater and the thermocouples from being damaged. The last quasi-steady state heat flux was then measured before the transition to film boiling was taken as the CHF. All of the measurements were taken only for increasing heat flux, and the effects of hysteresis were not examined.

2.3. Honeycomb porous plates

Fig. 2 shows the honeycomb porous plate used in the present study, and a micrograph of its structure is shown on the right-hand side of the figure. The honeycomb porous plate, which is commercially available, was used as a filter for purifying exhaust gases from combustion engines. The constituting ingredients consist of $CaO{\cdot}Al_2O_3$ (30–50 wt.%), fused SiO_2 (40–60 wt.%), and TiO_2 (5–20 wt.%). The wall thickness δ_s of the grid, the vapor escape channel width d_v, and the diameter of the honeycomb porous plate are 0.4 mm, 1.3 mm, and 30 mm, respectively. Therefore, the aperture rate is 0.55. Boling heat transfer experiments were conducted

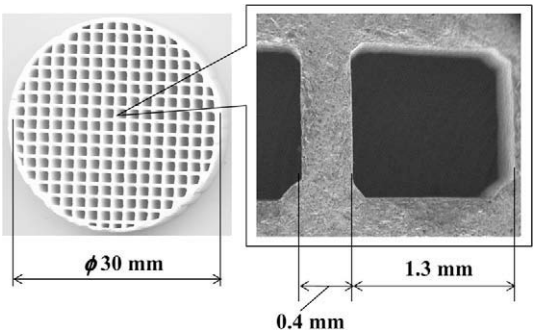

Fig. 2. Shape of the honeycomb porous plate.

using honeycomb porous plates having heights δ_h of 1.2 mm, 5.0 mm, and 10.0 mm, respectively. These wicks were attached to the top of boiling surface by pushing against the surface using a stainless steel wire net (mesh size: 10) without thermally conductive grease. The pore radius distribution of the honeycomb porous plates was measured by the mercury penetration porosimetry, which peaked at approximately 0.17 μm, as shown in Fig. 3. The average pore radius, the median pore radius, and the porosity of the honeycomb porous plates measured by porosimetry are 0.037 μm, 0.13 μm, and 24.8%, respectively.

2.4. Uncertainty analysis

The individual standard uncertainties are combined to obtain the estimated standard deviation of the results, which is calculated using the law of propagation of uncertainty (Taylor and Kuyatt (1993)).

The uncertainties of heat flux q, superheat ΔT_{sat}, and heat-transfer coefficient h are evaluated in the following equations, respectively.

$$\Delta q = \sqrt{\left(\frac{\partial q}{\partial \lambda}\Delta\lambda\right)^2 + \left(\frac{\partial q}{\partial \delta}\Delta\delta_1\right)^2 + \left(\frac{\partial q}{\partial T_1}\Delta T_1\right)^2 + \left(\frac{\partial q}{\partial T_2}\Delta T_2\right)^2} \quad (1)$$

$$\Delta(\Delta T_{sat}) = \sqrt{\left(\frac{\partial(\Delta T_{sat})}{\partial q}\Delta q\right)^2 + \left(\frac{\partial(\Delta T_{sat})}{\partial T_1}\Delta T_1\right)^2 + \left(\frac{\partial(\Delta T_{sat})}{\partial \delta_2}\Delta\delta_2\right)^2 + \left(\frac{\partial(\Delta T_{sat})}{\partial \lambda}\Delta\lambda\right)^2} \quad (2)$$

$$\Delta h = \sqrt{\left(\frac{\partial h}{\partial(\Delta T_{sat})}\Delta(\Delta T_{sat})\right)^2 + \left(\frac{\partial h}{\partial q}\Delta q\right)^2} \quad (3)$$

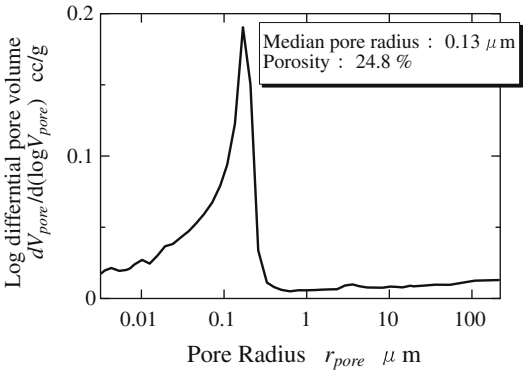

Fig. 3. Pore radius distribution of test porous media.

where T_1 and T_2 are the temperatures at TC1 and TC2, respectively, λ is the thermal conductivity of the copper evaluated at the arithmetic mean value of T_1 and T_2, δ_1 is the distance between TC1 and TC2, and δ_2 is the distance between TC1 and boiling surface.

Table 1 shows the example of results in the relative uncertainties calculated from Eqs. (1) to (3). As shown in the table, relative uncertainties depend on the experimental conditions, and the relative uncertainties tend to become smaller with the increase in the heat flux.

3. Experimental results and discussion

3.1. Effect of micro-pores and vapor escape channels on the CHF

Fig. 4 shows the boiling curves for different structures of porous plates, i.e., a honeycomb porous plate, a honeycomb solid plate without micro-pores, which was fabricated by impregnating a honeycomb porous plate with adhesive, and a solid porous plate without vapor escape channels, having a height of 5.0 mm. Experiments using a honeycomb solid plate without micro-pores and a solid porous plate without vapor escape channels was carried out in order to clarify the effect of a capillary suction and the effect of vapor channels to avoid an excessive pressure increase in the porous structure on the CHF, respectively. The arrows indicated in Fig. 4 correspond to the CHF condition. As clearly seen from Fig. 4, the CHF for honeycomb porous plate is 1.4 MW/m^2, which is approximately 1.6 times and four times that of the honeycomb solid plate (0.88 MW/m^2) and solid porous plate (0.36 MW/m^2), respectively. These results signify that micro-pores provide strong capillary suction and vapor escape channels are necessary to improve the CHF. That is, the CHF enhancement is attributed to the automatic liquid supply due to capillary action and the reduction of the liquid–vapor counter-flow resistance adjacent to the heated surface due to the separation of the liquid and vapor flow by the honeycomb structure.

3.2. Effects of the heights in honeycomb porous plates δ_h on the CHF and heat-transfer coefficient h

The saturated boiling curves of the honeycomb porous plates at different heights and that of a plain surface are compared in Fig. 5. As shown clearly in the figure, the CHF is increased dramatically with the decrease of heights in the honeycomb porous plates. In particular, a honeycomb porous plate for a height of 1.2 mm can remove the heat flux of 2.5 MW/m^2, which is approximately 2.5 times that of a plain surface (1.0 MW/m^2).

Fig. 6 shows the relationship between the CHF and heights of honeycomb porous plates. The solid line and the dash-dotted line in this figure indicate the viscous-drag limit predicted by Eq. (9) and the hydrodynamic limit calculated by the model proposed by Liter and Kaviany (2001), respectively. Comparison of these results will be discussed later. As seen in this figure, the measured CHF increases with the decrease of the height in the honeycomb porous plates.

Comparing measured heat-transfer coefficients for different heights of honeycomb porous plates with that of a plain surface, as shown in Fig. 7, the difference in the values of heat-transfer

Table 1
The relative uncertainties of the experimental measurements.

q (MW/m^2)	ΔT (K)	h (W/(m^{2}K))	$\Delta q/q$ (%)	$\Delta T_{sat}/T_{sat}$ (%)	$\Delta h/h$ (%)
0.5	17	28,000	13.2	6.0	14.5
1.2	28	41,000	5.6	3.7	6.7
1.7	36	46,000	4.1	3.1	5.1
2.3	47	49,000	3.1	2.4	3.9

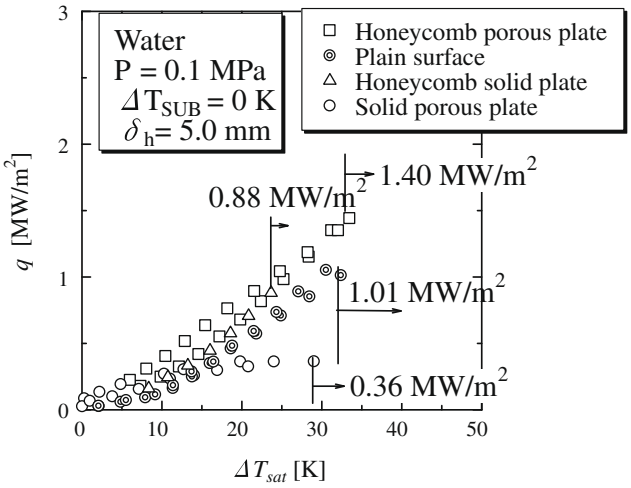

Fig. 4. Boiling curves for different structures of porous plates.

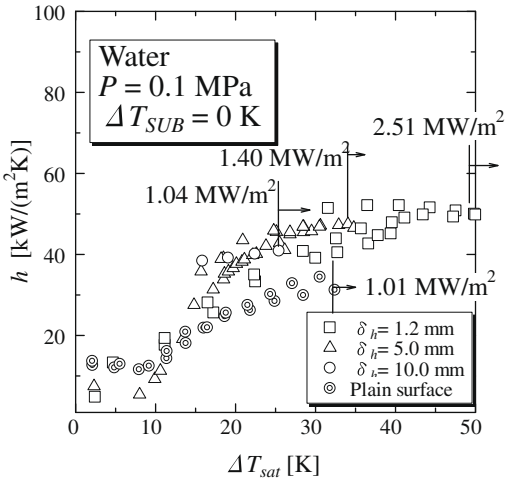

Fig. 7. Heat-transfer coefficients for honeycomb porous plates of different heights.

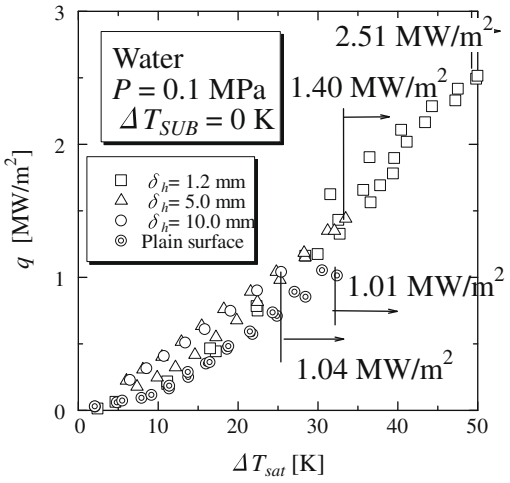

Fig. 5. Boiling curves for honeycomb porous plates of different heights.

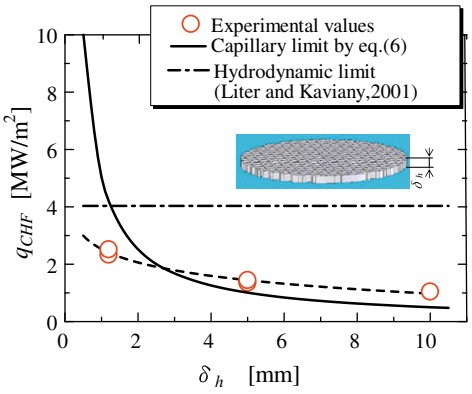

Fig. 6. Relationship between q_{CHF} and height of the honeycomb porous plate.

coefficients between different heights (δ_h = 1.2 mm, 5.0 mm, and 10.0 mm) of honeycomb porous plates are not obvious, although they are just slightly larger than that of a plain surface.

As mentioned above, the three possible CHF enhancement mechanisms for the use of porous media have been considered. The first is the capillary suction effect. The second is an extended surface area effect, and the third is the effect of a decrease in the flow-critical length scale, or the distance between vapor columns, which is regulated by the modulation in a porous layer, corresponding to Rayleigh-Tayer wavelength in Zuber's hydrodynamic model, as suggested by Liter and Kaviany (2001).

As shown in Fig. 6, the CHF increases significantly as the height of the honeycomb porous plate decreases, which indicates the decrease in the extended surface area. Moreover, considering the low thermal conductivity in the honeycomb porous plates and the thermal contact resistance between a honeycomb porous plate and a heated surface, the CHF enhancement mechanism in the present phenomena is not related to the extended surface area effect. The hydrodynamic liquid choking limit for the case less than the honeycomb porous plates height δ_h of approximately 1.2 mm is smaller than the calculated value by the present model as shown in Fig. 6. However, the hydrodynamic limit also may be unrelated to the mechanism in the CHF presented herein even in the case of the honeycomb porous plates height δ_h of 1.2 mm. The reason is discussed in detail in the next section. As a result, the CHF may be governed by the capillary suction effect. Therefore, it is assumed that the CHF occurs within the porous layer when the viscous drag surpasses the available capillary pumping.

In order to clarify the CHF mechanism, a simplified one-dimensional model, which is similar to the capillary limit model for a conventional heat pipe, applied to the phenomenon, and the calculated results are compared with the observed results.

3.3. The CHF model based on capillary limit

Fig. 8 shows a schematic diagram of the steam and water flows in a honeycomb porous plate. As shown in the figure, liquid is transported toward the heated surface within the porous medium by capillary force, and vapor generated in close vicinity to the heated surface escapes upward through the vapor channels. It is assumed that dryout inside the porous material in close to the heated surface does not occur, that is, the inside of the porous material is completely filled with water in order to simplify the model.

The CHF is considered to be achieved under conditions such that the maximum capillary pressure $\Delta p_{c,\max}$ is equal to the sum of the pressure losses along the vapor–liquid path in the following:

$$\Delta p_{c,\max} = \Delta p_l + \Delta p_v + \Delta p_a \tag{4}$$

where Δp_l and Δp_v are the frictional pressure drops caused by the liquid flow in the porous medium and the vapor flow through the

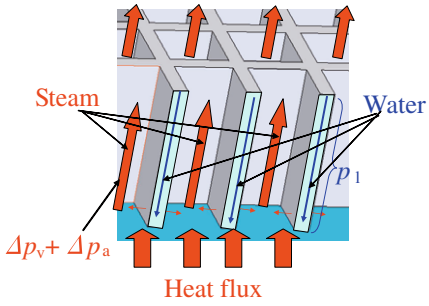

Fig. 8. Schematic diagram of steam and water flows in a honeycomb porous plate.

channels, respectively, and Δp_a is the accelerational pressure drop caused by phase change from liquid to vapor.

The maximum capillary pressure $\Delta p_{c,\max}$ can be calculated by

$$\Delta p_{c,\max} = \frac{2\sigma}{r_{eff}} \tag{5}$$

where r_{eff} is the effective pore radius, and σ is the surface tension.

The pressure drop Δp_l using Darcy's law is expressed as

$$\Delta p_l = \frac{\mu_l Q_{\max} \delta_h}{K A_W \rho_l h_{fg}} \tag{6}$$

where μ_l is the viscosity of the liquid, $Q_{\max}$ is the maximum heat transfer rate, δ_h is the height of the honeycomb porous plates, K is the permeability, ρ_l is the density of a liquid, A_w is the contacted area of the honeycomb porous plate with the heated surface, and h_{fg} is the latent heat of vaporization.

The vapor pressure drop Δp_v in a laminar incompressible flow (Reynolds number for the vapor flow in the present work is less than approximately 850) is given by

$$\Delta p_v = \frac{32 \mu_v \delta_h Q_{\max}}{\rho_v n d_v^4 h_{fg}} \tag{7}$$

where μ_v is the viscosity of the vapor, and n is the number of the vapor escape channels on the heated surface.

The accelerational pressure drop can be obtained as

$$\Delta p_a = \frac{\rho_v}{2} \left(\frac{Q_{\max}}{\left(\rho_v n d_v^2\right) h_{fg}} \right)^2 \tag{8}$$

The following CHF is obtained by substituting Eqs. (5)–(8) into Eq. (4) and using the heated surface area A (approximately 7.07 cm^2), as follows:

$$q_{CHF} = \frac{Q_{\max}}{A} = \frac{-B + \sqrt{B^2 + 4C(2\sigma/r_{eff})}}{2AC},$$
$$B = \frac{\mu_l \delta_h}{K A_W \rho_l h_{fg}} + \frac{32 \mu_v \delta_h}{\rho_v n d_v^4 h_{fg}}, \quad C = \frac{\rho_v}{2} \left(\frac{1}{\left(\rho_v n d_v^2\right)} h_{fg} \right)^2 \tag{9}$$

where the permeability K and the effective pore radius r_{eff} were determined by experimental measurements ($K = 2.4 \times 10^{-14}$ m^2, $r_{eff} = 1.6$ μm).

As shown in Fig. 6, both the measured values and the values calculated by Eq. (9) increase as the height of honeycomb porous plate decreases. A measured value in Fig. 6, however, is smaller than a calculated one for the case of honeycomb porous plate height δ_h of 1.2 mm, which may be attributed to the assumption that the dryout does not occur inside the porous material in the vicinity of the heated surface. For the case of dryout occurrence inside the porous material, the frictional pressure drop caused by the vapor flow through the thin porous wall should be added to right-hand side of Eq. (4), resulting in the decrease of the CHF. Taking into above discussion consideration, the limiting mechanism in this case is also considered to be not the hydrodynamic limit but capillary limit although CHFs predicted by the capillary limit and hydrodynamic limit is almost the same for the honeycomb porous plates height δ_h of 1.2 mm in Fig. 6, as pointed out in the previous section. Moreover, considering the observed values, the CHF can be explained roughly by the one-dimensional model, which means two-dimensional effect is not significant on the CHF, the cooling technology using honeycomb porous plates presented herein may apply to large heated surface area cooling with high heat flux in the saturated pool boiling.

3.4. Relationship between vapor escape channel widths d_v and predicted CHFs

The CHF performance using honeycomb porous plates depends on the pore radius r_{eff}, the permeability K, the height of the porous media δ_h, the vapor escape channel width d_v, and the wall thickness δ_s of the porous medium between vapor escape channels. These parameters must be optimized in order to achieve the maximum CHF. In particular, the effect of the vapor escape channel width d_v on the CHF is examined in the following three cases, i.e., (a) $\Delta p_{c,\max} = \Delta p_l + \Delta p_v + \Delta p_a$, (b) $\Delta p_{c,\max} = \Delta p_l + \Delta p_v$, and (c) $\Delta p_{c,\max} = \Delta p_l$.

Fig. 9 shows the CHF values calculated as a function of the vapor channel width d_v, for the honeycomb porous plates height δ_h of 1.2 mm and 5.0 mm in the above cases (a) to (c), together with the measured results. The wall thickness δ_s between the neighboring vapor channels was fixed to 0.4 mm, which is equal to that of the tested plates. Taking the predicted values into consideration, the CHF_s in the above three cases ((a) to (c)) are almost the same for the case of more than the channel width d_v of 0.3 mm, it is obvious that the CHFs for the region is dominated by the frictional pressure loss Δp_l of liquid flow inside the porous medium. Moreover, considering that the difference of the value between cases (a) and (b) is small, accelerational pressure loss does not influence dramatically on the CHF. The CHF increases significantly with the decrease in the width of the vapor channel at larger widths and decreases markedly at smaller widths. The increase in the CHF with the reduction of the channel width at large widths is due to the increase in the contact area of the porous plate with the heat transfer surface area. The increase in the contact area reduces the mass flux and pressure drop of the liquid flow in the porous wall, resulting in the higher allowable evaporation rate over the entire heat transfer surface. Whereas, smaller channel widths cause a significant increase in the pressure drop for the vapor flow in the escape channel, which results in a smaller CHF. Because of the difference in the

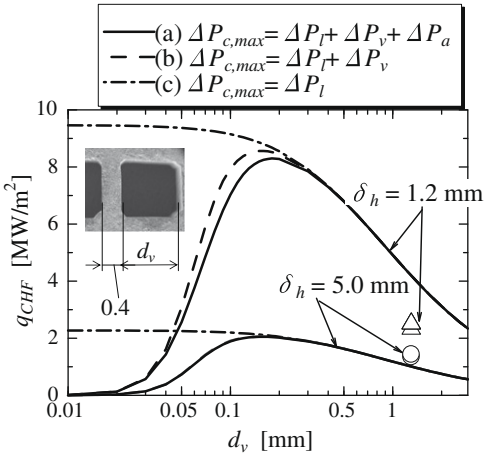

Fig. 9. q_{CHF} as a function of d_v.

limiting mechanisms, the calculated CHF shows the maximum values, which are approximately 8.0 MW/m^2 and 2.0 MW/m^2 at the channel width d_v of approximately 0.16 mm for the plate thicknesses δ_h of 1.2 mm and 5.0 mm, respectively. The calculated results suggest that the optimum width for maximizing the CHF would be much smaller than that of the tested plates.

3.5. Generalization of the relationship between the CHF and the specification of the honeycomb porous plate

The frictional pressure drops Δp_l in Eq. (4) plays a significant effect on the CHF for the case of more than the channel width d_v of 0.3 mm, as pointed out in the previous section. Therefore, the universal relationship between the CHF and the specification of the honeycomb porous plate (r_{eff}, K, δ_h, n, and d_v) for the dominated region by viscous force in liquid flow is discussed using the appropriate non-dimensional parameter.The non-dimensional CHF q^*_{CHF} is defined as the ratio of viscous force in the liquid flow to surface tension in the following:

$$q^*_{CHF} \equiv \frac{q_{CHF}\mu_l}{\rho_l \sigma h_{fg}} \tag{10}$$

Eq. (4) is rewritten by substituting Eqs. (5)–(8) and (10) into (4), as follows:

$$\frac{2}{r_{eff}A} = \frac{\delta_h}{KA_W} q^*_{CHF} + \frac{32\left(\frac{\mu_v}{\mu_l}\right)\delta_h}{\left(\frac{\rho_v}{\rho_l}\right) n d_v^4} q^*_{CHF} + \frac{1}{2}\frac{\rho_v \sigma A}{\left(\frac{\rho_v}{\rho_l} n d_v^2 \mu_l\right)^2} (q^*_{CHF})^2 \tag{11}$$

The non-dimensional CHF q^*_{CHF} is obtained by solving Eq. (11).

On the other hand, for the region governed by viscous force in the liquid flow, q^*_{CHF} is expressed simply by neglecting second and third terms in the right-hand side of Eq. (11) as

$$q^*_{CHF} = \frac{2K}{r_{eff}\delta_h}\left(\frac{A_W}{A}\right) \tag{12}$$

As seen clearly from Eq. (12), this equation indicates the non-dimensional parameter of the specification in the honeycomb porous plate.

Fig. 10 shows q^*_{CHF} as a function of non-dimensional parameter $\frac{2K}{r_{eff}\delta_h}\left(\frac{A_W}{A}\right)$ of the specification in the honeycomb porous plate. The solid line and the broken line are calculated from Eqs (11) and (12), respectively.

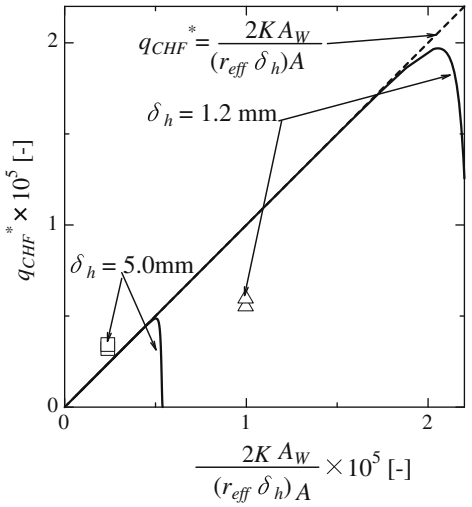

Fig. 10. q^*_{CHF} as a function of $\frac{2K}{r_{eff}\delta_h}\left(\frac{A_W}{A}\right)$.

The agreement between solid and broken line in Fig. 10 means the frictional pressure drop Δp_l affects the CHF significantly. Furthermore, it is possible to generalize the relation between q_{CHF} and the specifications of the honeycomb porous plate (r_{eff}, K, δ_h, n, and d_v) by using q^*_{CHF} and $\frac{2K}{r_{eff}\delta_h}\left(\frac{A_W}{A}\right)$ as shown in Fig. 10.

4. Conclusions

Enhancement of the critical heat flux in pool boiling by the attachment of a honeycomb-structured porous plate on the heated surface was investigated experimentally using water under the saturated boiling conditions. The following conclusions were obtained:

1. The porous plate must have micro-pores with strong capillary suction and vapor escape channels in order to enhance the CHF.
2. The saturated pool-boiling CHF is shown experimentally to become approximately 2.5 times by the attachment of a honeycomb porous plate, compared to that of a plain surface (approximately 1.0 MW/m^2) with 30 mm of heated surface diameter, which is relatively large.
3. The CHF values predicted by the one-dimensional capillary-limit model agree qualitatively with the measured values. The arrangement of honeycomb porous plates on the heated surface may remove the high heat flux over the large heated surface area. According to the model, the optimum vapor channel width for the CHF enhancement is approximately 0.16 mm, and the predicted maximum CHF reaches approximately 8 MW/m^2 for the honeycomb porous plate having a height of 1.2 mm.

Acknowledgement

This study was supported in part by the Kurata Memorial Hitachi Science and Technology Foundation.

References

Arik, M., Bar-Cohen, A., You, S.M., 2007. Enhancement of pool boiling critical heat flux in dielectric liquids by microporous coatings. Int. J. Heat Mass Transfer 50, 997–1009.
Bar-Cohen, A., 1993. Thermal management of electronic components with dielectric liquids. JSME Int. J. 36, 1–25.
Chang, J.Y., You, S.M., 1997. Enhanced boiling heat transfer from micro-porous surfaces: effects of a coating composition and method. Int. J. Heat Mass Transfer 40, 4449–4460.
Coursey, J.S., Kim, J., Boudreaux, P.J., 2005. Performance of graphite foam evaporator for use in thermal management. J. Electron. Packaging 127, 127–134.
Honda, H., Wei, J., 2004. Enhanced boiling heat transfer from electronic components by use of surface microstructures. Exp. Therm. Fluid Sci. 28, 159–169.
Hwang, G.S., Kaviany, M., 2006. Critical heat flux in thin, uniform particle coatings. Int. J. Heat Mass Transfer 49, 844–849.
Lienhard, J.H., Dhir, V.K., Riherd, D.M., 1973. Peak pool boiling heat-flux measurements on finite horizontal flat plates. J. Heat Transfer 95, 477–482.
Liter, S.G., Kaviany, M., 2001. Pool boiling CHF enhancement by modulated porous layer coating: theory and experiment. Int. J. Heat Mass Transfer 44, 4287–4311.
Malyshenko, S.P., 1991. Features of heat transfer with boiling on surfaces with porous coatings. Therm. Eng. 38, 38–45.
Mugha, M.P., Plumb, O.A., 1996. An experimental study of boiling on a wicked surface. Int. J. Heat Mass Transfer 39, 771–777.
Stubos, A.K., Buchlin, J.M., 1999. Enhanced cooling via boiling in porous layers: the effect of vapor channels. J. Heat Transfer 121, 205–210.
Semenic, T., Lin, Y.Y., Catton, I., Sarraf, D.B., 2008. Use of biporous wicks to remove high heat fluxes. Appl. Therm. Eng. 28, 278–283.
Taylor, B.N., Kuyatt, C.E., 1993. Guidelines for evaluation and expressing the uncertainty of NIST measurement results, NIST Tech. Note 1297, 1–20.
Webb, R.L., 1983. Nucleate boiling on porous coated surfaces. Heat Transfer Eng. 4, 71–82.
Wu, W., Du, J.H., Hu, X.J., Wang, B.X., 2002. Pool boiling heat transfer and simplified one-dimensional model for prediction on coated porous surfaces with vapor channels. Int. J. Heat Mass Transfer 45, 1117–1125.